INTERNATIONAL JOURNAL FOR NUMERICAL METHODS IN FLUIDS, VOL. 10, 305–325 (1990)

COMBINED RADIATION AND NATURAL CONVECTION IN A RECTANGULAR CAVITY WITH A TRANSPARENT WALL AND CONTAINING A NON-PARTICIPATING FLUID

M. BEHNIA, J. A. REIZES AND G. DE VAHL DAVIS

School of Mechanical and Industrial Engineering, University of New South Wales, Kensington, NSW, Australia 2033

SUMMARY

This paper describes a numerical method for the study of combined natural convection and radiation in a rectangular, two-dimensional cavity containing a non-participating (i.e. transparent) fluid.

One wall of the cavity is isothermal, being heated either by solar radiation or independently. The opposite wall is partially transparent, permitting radiation exchanges between the cavity and its surroundings and/or the Sun; that wall also exchanges heat by convection from its external surface to the surroundings. The other two walls are adiabatic: convection and radiation there are balanced, so that there is no heat transfer through those walls.

The equations of motion and energy are solved by finite difference methods. Coupled to these equations are the radiative flux boundary conditions which are used to determine the temperature distribution along the non-isothermal walls. A two-band radiation model has been employed.

Results are presented for a square cavity with a vertical hot wall at 150 °C, the ambient at 20 °C and $10^4 \leq Ra \leq 3 \times 10^5$, in the absence of direct insolation. The effects on the flow and heat transfer in the cavity of radiation and external convection have been examined. More extensive results will be presented in subsequent papers.

KEY WORDS Natural convection Radiation Solar collector Finite differences

INTRODUCTION

Because of its many engineering applications, natural convection in enclosures has been the topic of much research, particularly in the last two decades. Comprehensive reviews by Ostrach[1,2] and Catton[3] give an account of nearly half a century of work. The importance of flow structure and heat transfer processes in double-pane windows, solar collectors, double-wall insulation, nuclear reactor insulation, ovens and rooms has been the stimulus for much research in the area.

Buoyancy-driven natural convection in differentially heated upright cavities with adiabatic ends has become the classical research problem which has been extensively studied experimentally, analytically and numerically in order to gain a better understanding of the governing processes. Experimental research has produced many correlations for heat transfer and some information about the flow field through visualization techniques. The investigations by Arnold *et al.*,[4] Hollands *et al.*,[5] Randall *et al.*[6] and ElSherbiny *et al.*[7] are typical and important examples. Elder,[8] Vest and Arpaci,[9] Hart,[10] Morrison and Tran,[11] Seki *et al.*[12] and Schinkel[13] described further details of the flow revealed by visualization.

A large number of numerical studies of the problem have also been reported. The submission of some 37 contributions to a comparison exercise[14] gives an indication of the amount of interest in the numerical study of this problem.

0271–2091/90/030305–21$10.50

Received 29 January 1988
Revised 27 April 1989

The problem has usually been simplified to a study of cavities which have isothermal hot and cold boundaries. This has resulted partly from experimental difficulties associated with more complex boundary conditions, and partly because understanding of the internal convective processes has been the main goal of the research. In fact this has been done to such an extent that more realistic boundary conditions have been almost forgotten. However, many real physical situations, such as solar collectors and double-glazed windows, do not conform to such simple models. It follows that other types of boundary conditions need to be considered. To this end a numerical model in which different types of boundary conditions can be implemented is more versatile and may therefore be more attractive than laboratory or field experiments.

Since the main focus of most studies has been on buoyancy-driven natural convection in the cavity, the other modes of heat transfer and other interaction with the internal convection have usually not been considered. Because of engineering interest in natural convective flows which are affected by radiation heat transfer from high-temperature sources—e.g. fires in rooms or combustion processes—there have been some studies of such situations, for example by Larson and Viskanta,[15] Larsen,[16] Lloyd *et al.*[17] and Chang *et al.*[18]. Lauriat[19] has considered convection in an insulated enclosure, including the effects of long-wave radiation. However, in none of these studies have the authors considered all of the factors which we have included, namely both short- and long-wave radiation, two-dimensional natural convection, the calculation of local radiation view factors and, with solar collector applications in mind, with one transparent boundary.

In a natural convective process the radiative heat transfer may affect the temperature field—and hence the flow field—directly through absorption and emission processes within the fluid. This effect may be negligibly small, for example if the fluid is dry (or fairly dry) air. Radiation may also have an effect on the temperature field indirectly through an impact upon the temperature distribution on the solid boundaries. In a solar collector or double-pane window, radiation is transmitted and absorbed by the boundaries and may influence the convective flow patterns. Also, emission of radiation by the boundaries as well as radiative interaction between them have an important bearing on the boundary temperatures, although here—unlike in combustive processes—the temperature is not regarded as radiatively high. Because of the inherent coupling in natural convection between the thermal and flow fields through the buoyancy effects, the temperature changes on the boundaries caused by the radiative heat transfer can have a stronger consequence than might be expected.

A numerical model of a two-dimensional vertical or inclined rectangular cavity, filled with a radiatively non-participating fluid, with internal and external radiative heat exchanges, external convection and radiation from an external source has been developed and is described here. The cold boundary is taken to be a transparent 'window' whose temperature is determined from a heat balance with all modes of heat transfer properly taken into account. The computer program is so structured that all the radiative transfer computation routines can be bypassed so that the effect of neglecting radiation can be determined. Also, for comparison purposes, isothermal hot and cold boundary conditions with no radiative effects can be simulated with the same program.

The main purpose of this paper is to describe the methodology adopted. To illustrate the use of the program, some results are presented for a square cavity with convection on the outside of the cold boundary and also with no convective heat transfer there (as would occur, for example, if the cavity were in outer space or if external natural convection could be regarded as negligible). It is shown that even at the moderate temperatures considered here, the radiative mode of heat transfer is important and that the neglect of this mode of energy transfer and of external convection alters the flow and thermal fields and leads to significant differences in the heat transfer.

ANALYSIS

Physical model and assumptions

The rectangular, air-filled enclosure shown in Figure 1 has its third dimension (not shown in this figure) horizontal, normal to the plane of the paper, and much longer than the other dimensions, so that a two-dimensional flow is assumed to exist. All the walls are stationary and impermeable; no-slip conditions exist at them. The left face of the cavity—the hot wall—is an isothermal hot surface opaque to radiation; the right face—the cold wall—is imperfectly transparent (i.e. some absorption of radiation may occur) with convection and conduction energy exchanges with the surroundings occurring on its outside surface. The upper and lower walls are adiabatic and opaque to radiation.

It is assumed that the confined fluid is Newtonian and that the Boussinesq approximation is valid: the fluid is incompressible with constant properties except for the linear variation of density with temperature in the buoyancy term of the momentum equation. All surfaces are taken to be grey diffuse reflectors and emitters of radiation and the confined air is assumed to be radiatively non-participating (which implies that its water vapour content is low).

The two-dimensional assumption really the applicability of the model to angles of inclination of the cavity less than about 30° from the vertical.[20] At greater angles, experimental studies have shown that longitudinal rolls—i.e. rolls with their axes aligned up the slope—may form. However, these rolls, related to the three-dimensional instabilities which occur in Rayleigh–Benard convection, are weak in comparison with the main circulation and contribute relatively little to the overall heat transfer until the cavity is nearly horizontal.

The radiation calculations have been made using a two-band model: short- and long-wave. This implies that emission from the surfaces of the cavity is 'long'-wave radiation and that radiative flux of solar origin is 'short'-wave. The model is adequate to allow the separate effects of (external) solar and (local) low-temperature radiation to be incorporated without imposing an excessive computational burden. It also permits the surfaces to have different radiative properties

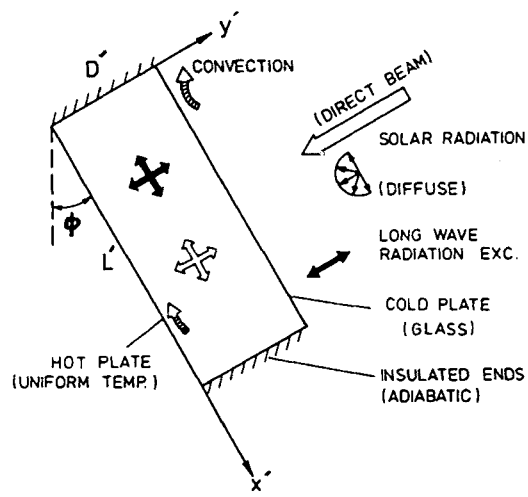

Figure 1. Physical model and the co-ordinate system

in each band. The treatment of the spectral nature of radiation and spectral integration are readily performed without serious loss of the details of the radiative energy transfers. The cold wall is considered to be sufficiently thin to allow the temperature difference across it due to conduction to be considered negligible, but thick enough to permit a fraction of the incident radiation to be absorbed.

Mathematical model

The equations governing the motion of the fluid in the cavity are those describing the conservation of mass, momentum and energy. The streamfunction–vorticity formulation (e.g. Reference 21) is used; the continuity equation is thereby automatically satisfied and the pressure eliminated as a solution variable.

It is usual to express the equations in non-dimensional form. However, since radiation is a function of the fourth power of absolute temperature, the temperature boundary conditions cannot be made non-dimensional in the usual manner which involves a temperature *difference*. Dimensional values of temperature must be used in the calculation of the radiative fluxes on the boundaries. Accordingly our results have not been generalized and actual temperatures are specified for each problem. (We could, alternatively, use a reference temperature, rather than a reference temperature difference, in the non-dimensionalization process. This, however, affects the definition of Rayleigh number and we have preferred to retain the conventional definition.)

Further, the only prescribed temperatures are those of the hot wall, the ambient and the background radiation exchange temperature. The Rayleigh (or Grashof) number is normally defined on the temperature difference between the hot and cold walls, which is here not known *a priori*; *Ra* is thus defined in terms of the temperature difference between the hot wall and the ambient air. An effective cavity Rayleigh number can be defined and calculated *a posteriori*.

The governing equations in dimensionless form are

$$\frac{\partial \zeta}{\partial t} + \frac{1}{Pr}\left(u\frac{\partial \zeta}{\partial x} + v\frac{\partial \zeta}{\partial y}\right) = \nabla^2 \zeta - Ra\left(\frac{\partial \theta}{\partial x}\sin\phi - \frac{\partial \theta}{\partial y}\cos\phi\right), \tag{1}$$

$$\frac{\partial \theta}{\partial t} + u\frac{\partial \theta}{\partial x} + v\frac{\partial \theta}{\partial y} = \nabla^2 \theta, \tag{2}$$

$$0 = \zeta + \nabla^2 \psi, \tag{3}$$

in which dimensionless variables are defined in accordance with

$$x = x'/D', \qquad y = y'/D', \qquad u = u'D'/\kappa,$$
$$v = v'D'/\kappa, \qquad \psi = \psi'/\kappa, \qquad \zeta = \zeta'D'^2/\kappa,$$
$$\theta = (T' - \tfrac{1}{2}[T'_h + T'_a])/(T'_h - T'_a), \qquad t = t'\kappa/D'^2.$$

Pr is the Prandtl number, ν/κ, and *Ra* is the Rayleigh number, $g\beta(T'_h - T'_a)D'^3/\kappa\nu$. The velocities u and v are related to the streamfunction by

$$u = \partial\psi/\partial y, \qquad v = -\partial\psi/\partial x. \tag{4}$$

Since the cavity is a closed surface, the boundary is a streamline and

$$\psi(0, y) = \psi(L, y) = \psi(x, 0) = \psi(x, 1) = 0, \tag{5}$$

in which $L = L'/D'$ is the aspect ratio of the cavity (see Figure 1). Because the tangential velocity

on each surface is zero,

$$\partial\psi/\partial x(0, y) = \partial\psi/\partial x(L, y) = \partial\psi/\partial y(x, 0) = \partial\psi/\partial y(x, 1) = 0, \tag{6}$$

The temperature of the hot wall is $\theta(x, 0) = 0{\cdot}5$.

The problem is overdetermined for the streamfunction equation (3), there are no boundary conditions for the vorticity transport equation (1) and there is (so far) only one boundary condition on the energy equation (2).

As described below, boundary values of the vorticity may be determined from equation (3), which at the boundary reduces to

$$\zeta_w = -(\partial\psi^2/\partial n^2)_w, \tag{7}$$

and from equation (6).

The temperatutre boundary conditions on the cold wall and the end walls are derived from energy balances. It should be noted that whilst there is no energy transfer *through* the end walls, there are energy exchanges there with both the other boundaries and with the fluid, so that the normal temperature gradient in the fluid adjacent to an adiabatic boundary is not zero. Each boundary will be treated in turn.

The energy balance at each point on the cold wall may be written

$$-k\left(\frac{\partial T'}{\partial y'}\right)_{y'=D} - h_0(T'_c - T'_a) + [\alpha_s(q'_{os} + q'_{is}) + \alpha_l(q'_{ol} + q'_{il}) - 2q'_e] = 0. \tag{8}$$

Here and below, k is the coefficient of thermal conductivity, h is the convective heat transfer coefficient from the cold wall to the surroundings, α, ρ and ε are the absorptivity, reflectivity and emissivity respectively, q' is the radiative flux, the subscripts c, e, i, o, l and s refer to the cold wall, emitted radiation, the inside and outside of the surface, and long- and short-wave incident radiation respectively, and

$$q'_e = \varepsilon\sigma T'^4. \tag{9}$$

We have included the effects of long-wave radiation emitted from the surroundings at an effective black body temperature T_e and incident on the exterior of the hot wall, so that

$$q'_{ol} = \sigma T'^4_e. \tag{10}$$

A similar energy balance on the upper and lower ends yields

$$k\left(\frac{\partial T'}{\partial x'}\right) + (-q'_e + \alpha_s q'_{is} + \alpha_l q'_{il}) = 0 \tag{11}$$

at both $x' = 0$ and $x' = L$.

Once the radiative fluxes have been determined, the temperatures of the boundaries can be calculated from equations (8)–(11) which couple the internal radiation and convection heat transfers on the end walls and which relate the internal convection and radiation heat transfers with the external convection and radiation energy transfers on the outside of the cold wall.

Radiative transfer equations

The finite difference mesh defines a set of elements on the boundaries. The radiation configuration factors between any pair of these elements must be determined.

The long-wave radiative heat flux, denoted by the subscript l, at any point z_m on the cavity surface m ($m = 1, 2, 3, 4$) can be written[22]

$$q'_l(z_m) = (\varepsilon_{ml}/\rho_{ml})[\sigma T'^4(z_m) - J'_l(z_m)], \tag{12}$$

in which $J'_l(z_m)$ is the radiosity:

$$J'_l(z_m) = \varepsilon_{ml}\sigma T'^4(z_m) + \rho_{ml}\sum_{\substack{j=1\\ j\neq m}}^{n}\int_{A_j} J'_l(z_j)K(z_m, z_j)\,\mathrm{d}A_j, \tag{13}$$

where $K(z_m, z_j)$ is the configuration factor (which includes the radiation properties of surface segment j). $T'(z_m)$ denotes the temperature of the mth segment, calculated as the average of the temperatures at each end of the segment.

If the upper and lower ends of the cavity are divided into N segments each, the cold wall is divided into M segments and the isothermal hot wall is treated as a single segment, the radiosity equations can be rewritten

$$J'_{jl} = \varepsilon_{jl}\sigma T'^4_j + \rho_{jl}\sum_{\substack{k=1\\ k\neq j}}^{M+2N+1} J'_k F_{jk}, \tag{14}$$

in which F_{jk} is the view factor between segments j and k. For a cavity bounded by plane surfaces, the view factor between any two points on the same surface is zero; this substantially reduces the number of terms on the right-hand side of equation (14). Furthermore, since a two-band radiation model is assumed and all the emitted radiation is in the long-wave band, the short-wave component of radiosity, J'_s, depends only on the geometry and the insolation. It is assumed that the direct insolation is normal to the hot and cold walls of the cavity; the hot wall short-wave radiosity is therefore

$$J'_{hs} = \rho_{hs}\left(\tau_{cs}q'_{os} + \sum_{\substack{k=1\\ k\neq h}}^{M+2N+1} J'_{ks}F_{kh}\right) \tag{15}$$

and at the ends it is

$$J'_{js} = \rho_{js}\sum_{\substack{k=1\\ k\neq j}}^{M+2N+1} J'_{ks}F_{kj}. \tag{16}$$

It follows from equations (15) and (16) that the short-wave radiosities need only be calculated once for a given geometry. The long-wave component J'_{jl}, however, needs to be evaluated at each stage of the calculation so that the radiosity

$$J'_j = J'_{js} + J'_{jl}. \tag{17}$$

The view factor between segments on any two walls can readily be shown to be given by one of the following four expressions:

$$F_{hj} = \frac{1}{2L}\{[1+(L-x_{j-1/2})^2]^{1/2} - [1+(L-x_{j+1/2})^2]^{1/2} + (1+x_{j+1/2}^2)^{1/2} - (1-x_{j-1/2}^2)^{1/2}\} \tag{18}$$

for the view factor between the isothermal hot wall and a segment j on the cold wall;

$$F_{jk} = \frac{1}{2\Delta y}\{[x_{k-1/2}^2 + (1-y_{j-1/2})^2]^{1/2} - [x_{k-1/2}^2 + (1-y_{j+1/2})^2]^{1/2} + [x_{k+1/2}^2 + (1-y_{j+1/2})^2]^{1/2} - [x_{k+1/2}^2 + (1-y_{j-1/2})^2]^{1/2}\} \tag{19}$$

for the view factor between a segment j on the upper (or lower) end and a segment k on the cold

window;

$$F_{jk} = \frac{1}{2\Delta y}\{[L^2 + (y_{j+1/2} - y_{k-1/2})^2]^{1/2} - [L^2 + (y_{j+1/2} - y_{k+1/2})^2]^{1/2} + [L^2 + (y_{j-1/2} - y_{k+1/2})^2]^{1/2} - [L^2 + (y_{j-1/2} - y_{k-1/2})^2]^{1/2}\} \quad (20)$$

for the view factor between a segment j on one end wall and a segment k on the other end; and

$$F_{jh} = \frac{1}{2\Delta y}[y_{j+1/2} - y_{j-1/2} + (L^2 + y_{j-1/2}^2)^{1/2} - (L^2 + y_{j+1/2}^2)^{1/2}] \quad (21)$$

for the view factor between a segment j on the upper (or lower) end and the hot wall.

The incident radiative heat transfers q'_{il} and q'_{is} in equations (8) and (11) can then be calculated from the radiosity by

$$q'_{il} = (J'_l - q'_e)/\rho_l, \qquad q'_{is} = J'_s/\rho_s.$$

The outside incident short-wave radiation q'_{os} is externally imposed (from the Sun) and the incident long-wave radiation q'_{ol} is calculated from the externally imposed radiation temperature.

SOLUTION OF THE EQUATIONS

The derivatives in the differential equations (1), (2) and (3) are approximated by central space differences and forward time differences. Since only the steady state solution is of interest, advantage is taken of the fast convergence rate of the false transient technique.[21] In this method a (false) time-dependent term $\partial\psi/\partial t$ is added to the left-hand side of equation (3), and the time derivatives in each of equations (1)–(3) are multiplied by false transient factors which effectively allow the rates of changes of the three solution variables ζ, θ and ψ to be independently controlled. These changes mean that the transient solution is incorrect but the steady solution to the false equations is the same as the solution to the true equations. The point of the changes is that they enable the inherent instability introduced by the FTCS scheme to be postponed to higher parameter values.

The resultant finite difference approximations (FDAs) are discretized with the Samarskii–Andreyev ADI scheme.[23]

The boundary values of the vorticity were calculated from Woods' second-order approximation[24] of equation (7) which is

$$\zeta_1 = -3\psi_2/(\Delta n)^2 - \zeta_2/2,$$

in which subscripts 1 and 2 refer to the boundary and the first mesh point in from the boundary; Δn is the mesh interval normal to the surface. The boundary conditions on the streamfunction are given by equation (5) and on the temperature by equations (8), (10) and (13). The derivatives of the temperature at the walls were approximated by three-point (second-order) backward or forward differences.

The solution is marched in time to steady state in the following order.

(a) From the boundary temperatures at the ith time step calculate the long-wave radiosities.
(b) Calculate the normal temperature gradients on the upper and lower walls and the cold wall from equations (11) and (8).
(c) Solve the FDA of the false transient form of equation (3) by ADI to obtain the internal temperature.

(d) Update the boundary value of the vorticity and solve the FDA of the false transient form of equation (1) to obtain the vorticity.
(e) Solve the false transient form of equation (2) to obtain the streamfunction.
(f) Compute the velocity field from the FDA of equation (4).
(g) Check whether the solution has converged (i.e. steady state reached); if not, return to (a).

Convergence to a steady solution, defined by obtaining an average, over all mesh points, of the relative changes in ψ, ζ and θ of less than 10^{-3}, was reached in a few hundred time steps (depending on the parameter values), requiring of the order of 2 min per 100 iterations on a VAX 11/785.

RESULTS

In the square cavity for which results are presented in this paper, various mesh sizes were tested to determine an adequate mesh for an accurate solution. A 41×41 mesh was found to be satisfactory in terms of both accuracy and computing economy for Rayleigh numbers up to 3×10^5. This is in very good agreement with the results of de Vahl Davis[25] who found that a 41×41 mesh yields solutions to pure natural convection in a square cavity with errors in Nusselt number less than 1% for $Ra \leq 10^6$.

The radiative properties, the external radiative sources, the external coefficient of convective heat transfer, the hot wall and ambient temperatures as well as the size and shape of the cavity all affect the thermal and flow fields inside the cavity. The results in this paper are limited to a square cavity containing air ($Pr = 0{\cdot}7$) with a hot wall temperature of 150 °C, an ambient temperature of 20 °C, an external convective heat transfer coefficient of 10 W m^{-2} °C^{-1}, which no sources of short-wave radiation (i.e. no direct sunlight) and with the surroundings at an effective black body temperature of 20 °C. All the surfaces were assumed to have an emissivity of 0·9 and the cold wall was assumed to be made of glass with the same internal and external radiation properties, namely a transmissivity of 0·05. The *cavity size* was varied so that $10^4 \leq Ra \leq 3 \times 10^5$. The external convection heat transfer coefficient used is appropriate to mild forced convection. The range of Rayleigh numbers was chosen because it is pertinent to solar collectors or oven windows (although the cavity geometry is not).

The emphasis in this paper is placed on the effects of long-wave radiation and external convection (R and EC) on the internal temperature distribution, the flow field and the heat transfer. Since the problem of a cavity with isothermal hot and cold walls and no radiation (henceforth called the 'standard' problem) has received much attention, the R and EC results will be compared with this standard problem. To compute the standard problem, the cold wall temperature was set equal to the average temperature of the cold wall in the respective R and EC problem.

To further illustrate the influence of external radiation and convection, as well of internal radiation, results are presented with either the external convective heat transfer coefficient set to zero or with the radiative effects removed.

A summary of the different calculations which were performed is given in Table I. A superscript asterisk on the run number denotes the 'standard' problem for which the cold surface, as well as the hot, is isothermal. The symbols R, EC and REC are used to indicate whether the effects of radiation, external convection or both have been included in the 'non-standard' problem. The numerical suffix to these symbols indicates the *overall* Rayleigh number.

As indicated above, the value of Ra^* (the cavity Rayleigh number for the standard problem) was computed using, for T'_c, the mean value of the cold wall temperature computed in the

Table I. Summary of results

Run	Ra	Ra^*	T_c(°C)	$\lvert\psi\rvert_{max}$
REC-10	10 000	5 800	74·8	4·199
REC-10*	—	5 800	74·8	3·921
EC-10	10 000	6 700	63·4	4·051
EC-10*	—	6 700	63·4	4·215
R-10	10 000	3 800	100·2	3·313
R-10*	—	3 800	100·2	3·103
REC-100	100 000	59 000	73·3	9·893
REC-100*	—	59 000	73·3	8·372
EC-100	100 000	67 000	62·5	8·304
EC-100*	—	67 000	62·5	8·640
R-100	100 000	39 000	99·0	9·158
RC-100*	—	39 000	99·0	7·551
REC-200	200 000	119 000	72·9	11·74
REC-200*	—	119 000	72·9	10·07
EC-200	200 000	135 000	62·3	9·928
EC-200*	—	135 000	62·3	10·43
R-200	200 000	79 000	98·6	10·75
R-200*	—	79 000	98·6	9·076
REC-300	300 000	178 000	72·7	13·04
REC-300*	—	178 000	72·7	11·17
EC-300	300 000	203 000	62·2	10·93
EC-300*	—	203 000	62·2	11·54
R-300	300 000	119 000	98·5	11·93
R-300*	—	119 000	98·5	10·07

R: radiation included.
EC: external convection included ($h = 10$ W m^{-2} °C^{-1}).
REC: both radiation and external convection included.
* 'Standard' problem with isothermal vertical boundaries.

corresponding non-standard problem; this differs from the Rayleigh number used in the R and EC problem, as defined in equation (1), and cannot be determined *a priori*. Once an average cold wall temperature has been determined from a converged R and EC solution, the standard problem can be attempted and a comparison made.

Low Rayleigh number

The streamlines for runs REC-10, EC-10 and R-10 (in which $Ra = 10\,000$) and for the corresponding isothermal cases are presented in Figure 2. In all figures, the hot wall is on the left and the fluid is circulating in a clockwise direction. Although at first sight it may appear that the general shape of the streamlines for all these runs is the same, a close examination indicates that there are significant differences. The streamlines for runs REC-10, EC-10 and R-10, unlike the corresponding standard runs, are not skew-symmetrical about the midpoint of the cavity. However, the departure from symmetry is small, so that the type of flow—but not the rate of circulation—is almost independent of the boundary condition. This can be explained by the fact that the shape of the isotherms, shown in Figure 3, indicates what is primarily a conduction regime in which the flow field is not greatly affected by the boundary condition.

The isotherms in Figure 3 show actual temperatures, rather than dimensionless temperatures, in oder to make comparisons possible. The lack of skew-symmetry is evident in the isotherms for

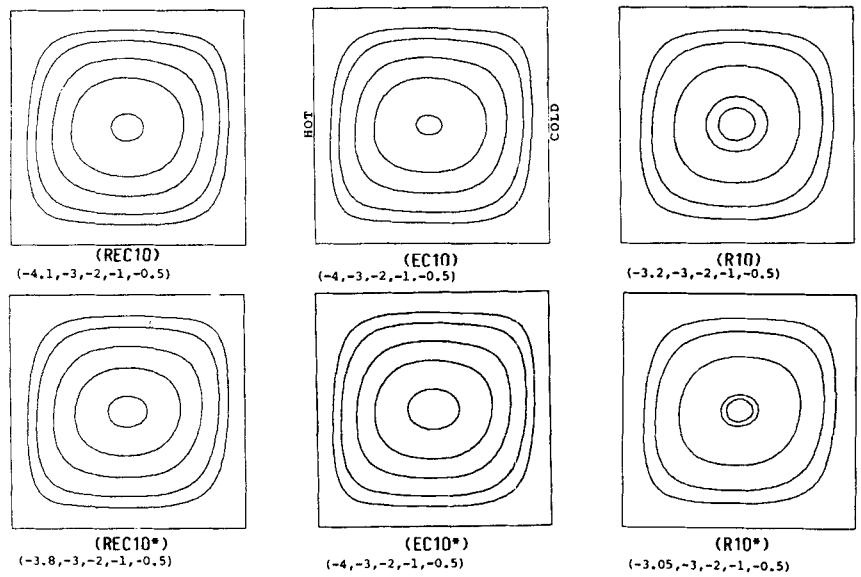

Figure 2. Streamlines for the runs REC-10, EC-10 and R-10, and for the corresponding standard runs (see Table I)

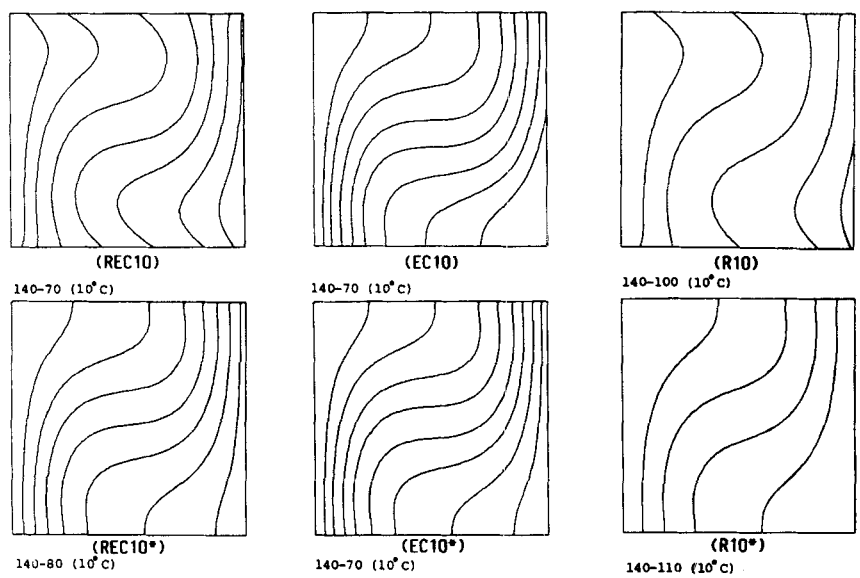

Figure 3. Isotherms for the flow fields shown in Figure 2

runs REC-10, EC-10 and R-10. Further, the shape of the isotherms for these runs is markedly different (in particular, runs REC-10 and R-10) from those of the corresponding isothermal solutions. Although the shape of the isotherms might appear similar for solutions EC-10 and EC-10*, in run EC-10 the isotherm closest to the cold wall intersects that boundary. This is consistent with the fact that the cold wall temperature is not uniform. The isotherms in the other two solutions (R-10 and R-10* series) indicates a similar trend. Further, the isotherms in solutions

REC-10 and R-10 are not normal to the *adiabatic* upper and lower end walls. This is because radiative energy exchanges there with the other surfaces are balanced by conduction *into the fluid.* There is no conduction into or through the end walls which are, in that sense, adiabatic.

High Rayleigh number

The streamlines for the solutions with $Ra = 300\,000$ (runs REC-300, EC-300 and R-100) and for the corresponding standard problems are presented in Figure 4. At this Rayleigh number the flow pattern inside the cavity of the R and EC problem is substantially different from that in the standard case, and the loss of skew-symmetry is apparent.

In run REC-300 the location of the cells is almost symmetrical, but at the centre of the left-hand cell $\psi = -13{\cdot}04$ whereas at the right-hand cell centre $\psi = -12{\cdot}74$. The streamfunction values at the two cell centres for run REC-300* are equal to $-11{\cdot}17$. Although the effective cavity Rayleigh number for run REC-300* is the same as that for run REC-300, radiative effects and external convection cause the two cells to move slightly further apart in case REC-300 than in the standard problem. In run EC-300, in which external radiation has been omitted so that the cold wall loses heat to the surroundings only by convection, the cell centres are at (0·4, 0·225) and (0·55, 0·775) whereas in the case of the the equivalent standard problem they are located at (0·375, 0·225) and (0·625, 0·775). This indicates that external convection has the opposite effect to radiative heat fluxes. Note that the neglect of radiation causes the cell centres to be close to the horizontal centreline of the cavity with a sharper bending of the streamlines in the inner core (compare streamlines for run REC-300 and EC-300). The cavity flow for $Ra = 300\,000$ is in the boundary layer regime and, unlike the conduction regime flows of Figure 2, it is strongly affected by the type of boundary condition.

The isotherms corresponding to the flow fields of Figure 4 are shown in Figure 5. Again, there is a considerable difference between the thermal field of runs REC-300, EC-300 and R-300 and the equivalent standard problem solutions. This difference is more marked in cases where radiation is

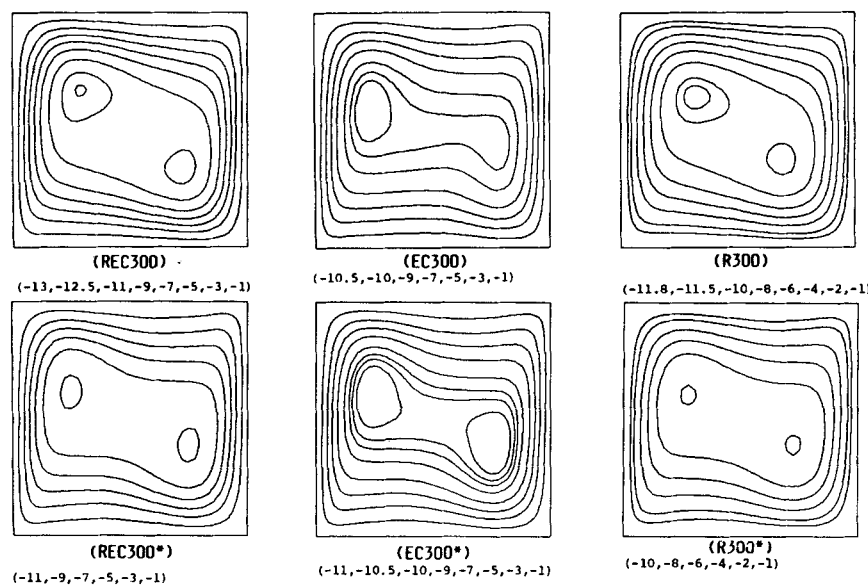

Figure 4. Streamlines for the runs REC-300, EC-300 and R-300, and for the corresponding standard runs (see Table I)

included in the calculations (indicated by a non-zero gradient at the upper and lower ends). The loss of skew-symmetry is also observed. The sharp bending of the isotherms (in the case of runs REC-300 and R-300) near the upperand lower ends (especially in the middle section of these walls) suggests that the fluid is being heated by the lower 'adiabatic' end and cooled by the upper 'adiabatic' end respectively. This heating and cooling effect leads to a stronger convective flow.

This effect can also be seen in the distribution of horizontal velocity along the vertical centreline (i.e. $v[x, 0{\cdot}5]$) of Figure 6. The dimensionless velocities for runs REC-300 and REC-300* have been plotted on the same graph to make comparison easier. The velocity near the end walls for run REC-300 is higher than for run REC-300*, although both cases have the same effective cavity Rayleigh number. The boundary layers on these walls are more distinct in run REC-300, indicating a stronger convective flow. Unlike the horizontal velocity profile in the

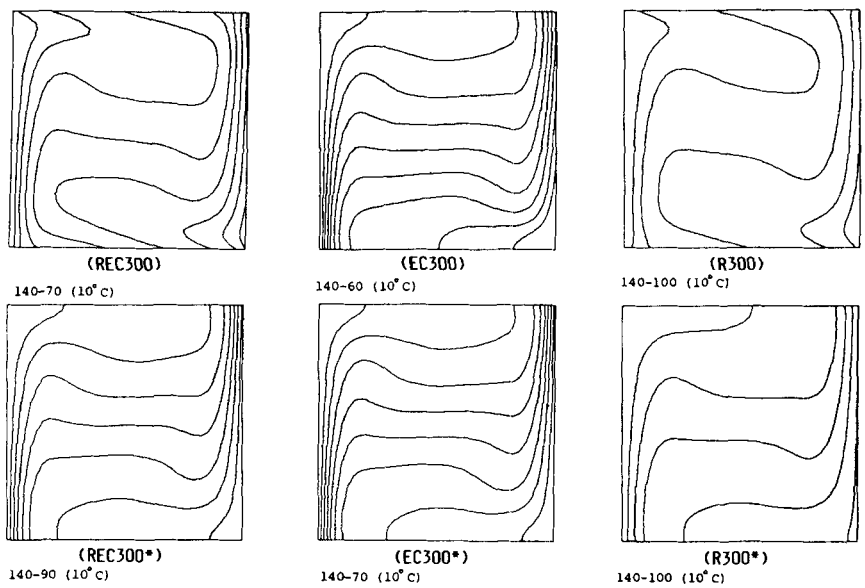

Figure 5. Isotherms for the flow fields shown in Figure 4

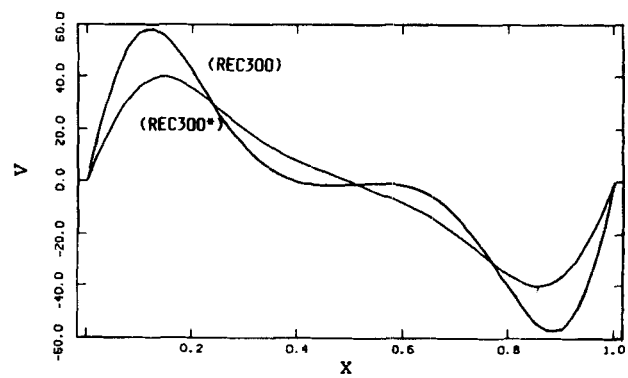

Figure 6. Horizontal velocity distribution along the vertical centreline for runs REC-300 and REC-300*

standard case, there is a pronounced stagnant core region in the solution with radiative transfer (run REC-300). The distributions of vertical velocity along the horizontal centreline (i.e. $u[0{\cdot}5, y]$) for these two solutions are nearly the same and have not been presented here.

To demonstrate the effects of radiative transfer and external convection on the horizontal velocity, a plot for runs REC-300, EC-300 and R-300 is given in Figure 7. It is evident that the profiles for runs REC-300 and R-300, in both of which radiation is included, are very similar. Interestingly enough, in the cse of run EC-300 in which radiation has not been included this velocity distribution is nearly the same as the standard case in Figure 6. Therefore the radiative transfer is the determining factor in the horizontal velocity distribution inside the cavity. Again, since the vertical velocity profiles for these three cases were not significantly different from each other, they are not shown here.

As mentioned earlier, the glass window (cold wall) is not isothermal so that its temperature is not uniform. The temperature distribution on this boundary is determined by the internal and external radiative exchanges as well as internal and external convection. Two typical cold wall temperature distributions are plotted in Figure 8 for Rayleigh numbers of 10^4 (run REC-10) and 3×10^5 (run REC-300). In both of these runs the radiative transfer was taken into account and the external convective heat transfer coefficient was 10 W m^{-2} °C^{-1}. There are temperature reversals near both the top and bottom of this wall. This is because of the radiative heating of the end

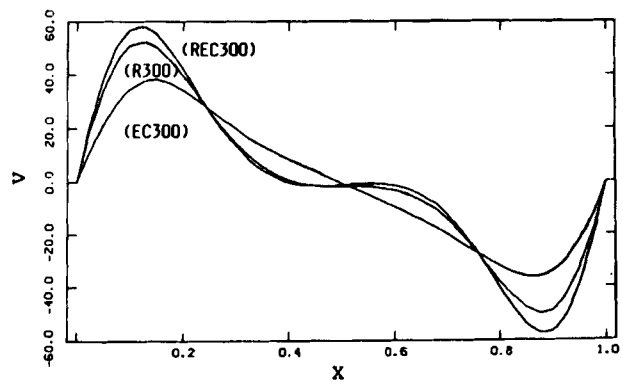

Figure 7. Horizontal velocity distribution along the vertical centreline for runs REC-300, EC-300 and R-300

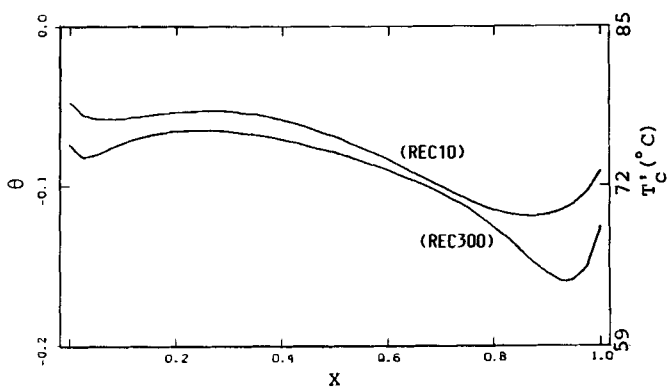

Figure 8. Temperature distribution along the cold wall for runs REC-10 and REC-300

sections of the cold wall by the adjacent upper or lower ends. The Rayleigh numbers for these two solutions are substantially different but the two temperature profiles are quite similar, especially away from the lower end. In fact the average temperature of the cold wall in run REC-10 is only 2·1 °C higher than that in case REC-300, suggesting that the cold wall temperature is not very greatly affected by the internal convective flow.

Intermediate Rayleigh number

The upper and lower end temperature distributions for the runs REC-200, EC-200 and R-200 ($Ra = 2 \times 10^5$) are shown in Figures 9(a) and 9(b) respectively. Whilst the removal of radiative effects results in a higher temperature for the upper end—compare the profiles for runs REC-200 and EC-200 in Figure 9(a)—the opposite occurs at the lower end—see Figure 9(b). From a standpoint of the end temperature prediction, the radiative effects result in a cooling of the top and a heating of the bottom. If the radiation is not included, the upper and lower end temperatures will be greatly overpredicted and underpredicted respectively. Furthermore, the external convective heat transfer has a determining effect on these temperatures (see Figures 9(a) and 9(b), curves (REC-200) and (R-200)). For the run R-200 ($h=0$) the upper end temperature is consistently higher than that of run REC-200 ($h=10\ \mathrm{W\,m^{-2}\,^{\circ}C^{-1}}$). An opposite trend is seen for the

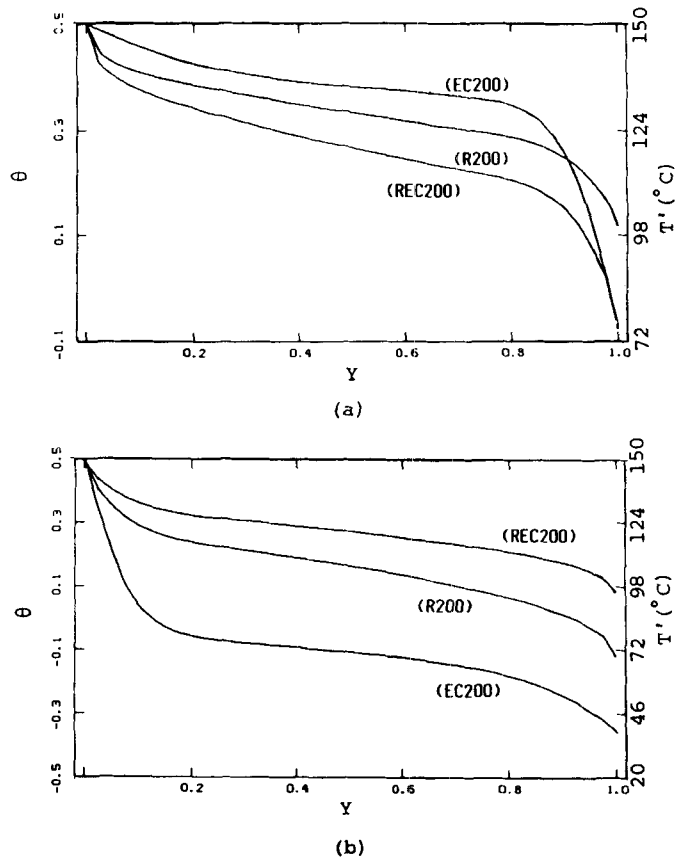

Figure 9. Temperature distribution along the end walls for runs REC-200, EC-200 and R-200: (a) upper end; (b) lower end

lower end—see Figure 9(b). The difference between the predicted end temperature distributions for these two cases is more significant at the lower than the upper end. The trend suggests that the external convective heat transfer has a cooling effect on the top end and a heating effect on the bottom end.

Strength of convection

External heat transfer affects the strength of the internal circulation, as measured by the maximum value of $|\psi|$. For cases involving only external convection, i.e. when external radiative effects are not included, the internal circulation is always weaker than in the corresponding isothermal case. The difference is small: for instance, it is only 3·9% between runs EC-100 and EC-100*. On the other hand, the inclusion of external radiation, with or without external convection, results in a stronger circulation than that which occurs in the correponding standard cases: for instance, the circulation in case REC-100 is 18·2% stronger than in case REC-100*. This indicates that if the cold wall were to be modelled as an isothermal surface at an effective average temperature T_c, with the radiative effects not properly accounted for, the circulation would be underestimated by 18·2% in this particular case. Furthermore, a comparison of runs M and N shows that even if the cold wall is not assumed isothermal and the external convective cold boundary is modelled properly, neglect of radiation would still lead to underprediction of internal circulation by 19·3% and of the average cold wall temperature by 10·5 °C (i.e. down from 72·7 °C for run REC-300 to 62·2 °C for run EC-300). It is interesting to note that whilst in run REC-300 (radiation included) the circulation is stronger than run EC-300 (radiation neglected), the effective cavity Rayleigh number is *smaller* for run REC-300, indicating that the radiative effects enhance the internal circulation in the cavity.

The external convective heat transfer also has a strong effect on the circulation inside the cavity. A comparison between the results of runs REC-300 ($h = 10\ \mathrm{W\ m^{-2}\ °C^{-1}}$) and R-300 ($h = 0$) shows that the cold wall temperature is 25·8 °C higher in the latter case and the circulation is 9·3% lower.

In summary: external convection weakens the internal circulation; radiation strengthens it; and in combination—at least for the parameter values used here—the overall effect is a strengthening of the internal circulation.

Heat flux calculation results

From an engineering and practical viewpoint, the rate of heat transfer across the cavity is a very important characteristic of the flow. The local convective heat flux $Q(x)$ in a horizontal direction at the hot (or cold) wall is given by

$$Q(x)_{\mathrm{conv}} = -(\partial\theta/\partial y)_{\mathrm{w}},$$

which was obtained using a three-point backward formula. The Nusselt number was calculated by integrating the local heat flux using Simpson's rule. It is again pointed out that the temperature is non-dimensionalized with $T'_h - T'_a$, except in the standard case which is based on $T'_h - T'_c$. Therefore, for comparison of the Nusselt numbers betweeen each solution and the corresponding standard case, the temperature non-dimensionalization must be based on the hot wall and the calculated average cold wall temperature T'_c. This adjustment yields a Nusselt number which is a measure of the convective heat transfer in the cavity.

For the cases in which radiative transfer is considered, a radiation Nusselt number (averaged along the wall) is defined as

$$Nu_{\mathrm{rad}} = (Q_{\mathrm{rad}}/Q_{\mathrm{conv}})\, Nu_{\mathrm{conv}},$$

in which Q_{rad} and Q_{conv} are the net radiative and convective heat transfer rates from the hot wall. The total heat transfer can be determined by a total Nusselt number (Nu_{tot}) which is the sum of the convective and radiative Nusselt numbers. For the sake of clarity, the Nusselt numbers based on the ambient temperature are shown with primes.

The internal convective local heat fluxes for runs REC-300 and REC-300* on the hot and cold walls are given in Figures 10(a) and 10(b) respectively. The Nusselt number in this figure is based on $T'_h - T'_c$. For both cases the effective cavity Rayleigh number (Ra^*) is the same (178 000). In the standard case (run REC-300*) the hot and cold wall Nusselt numbers are skew-symmetrical, as expected from a Boussinesq fluid and isothermal hot and cold side walls. There is no such symmetry in the case of solution REC-300. It is seen that an isothermal cold wall assumption results in an overprediction of local heat flux in the upper half of the cold wall and an underprediction in the lower half (Figure 10(b)); on the other hand, there is an opposite trend near the top and in the bottom half of the hot wall (Figure 10(a)). Thus if the local convective heat flux is of interest, the solutions based on the standard problem yield erroneous rates of heat transfer on the cold as well as the hot wall. The local hot wall convective heat flux for run REC-300 together with those for cases EC-300 and R-300 ($Ra = 3 \times 10^5$) are plotted in Figure 11. In this figure the Nusselt number is based on $T'_h - T'_a$. It is seen that except in the region near the top of the hot wall, the convective heat transfer rate from the wall is higher when radiation is neglected (compare curves REC-300 and EC-300). This difference near the bottom can be as high as 100%.

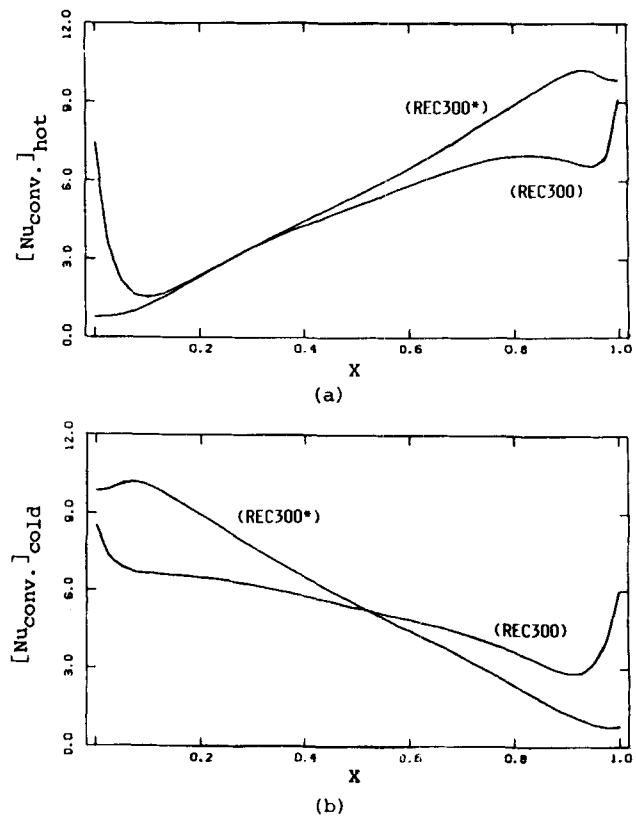

Figure 10. Local convective heat flux for runs REC-300 and REC-300*: (a) hot wall; (b) cold wall

The average hot wall Nusselt numbers for different Rayleigh numbers are plotted in Figures 12 and 13. In these figures the calculations from the runs in which radiation has been considered are given. The total Nusselt number (i.e. $Nu'_{rad} + Nu'_{conv}$) as well as the standard problem convective Nusselt number (Nu^*) are also given for comparison purposes. The same symbol has been used for the convective Nusselt number (Nu') and the corresponding one obtained from the standard solution (Nu^*). However, as explained earlier, the basis of the non-dimensionalization for the two are different. At a Rayleigh number of 2×10^5 the convective heat transfer from the hot wall accounts for only 33% of the total heat flux for $h = 10\ \mathrm{W\ m^{-2}\ °C^{-1}}$ compared with 29% for $h = 0$. This indicates that the radiative heat transfer from the hot wall for the runs shown here is the dominant heat transfer mode. It is interesting to note that the lines of the total Nusselt number and the standard problem convective Nusselt number are very nearly parallel, so that the total Nusselt number could be obtained by multiplying the standard solution convective Nusselt number at the same Rayleigh number by a constant.

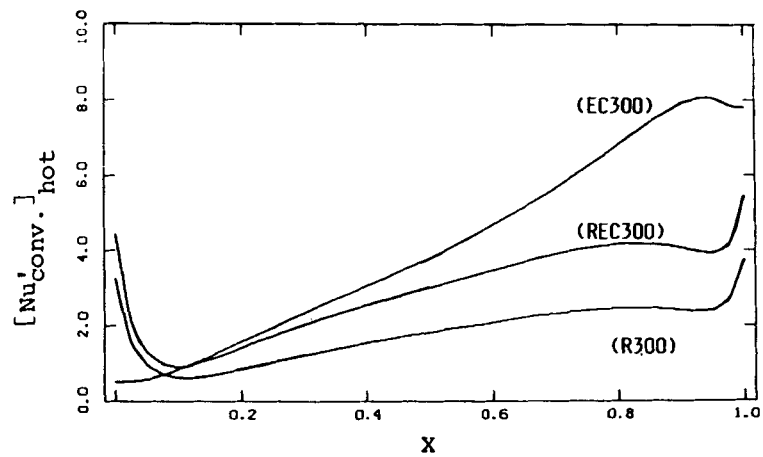

Figure 11. Local heat flux (based on $T'_h - T'_a$) along the hot wall for runs REC-300, EC-300 and R-300

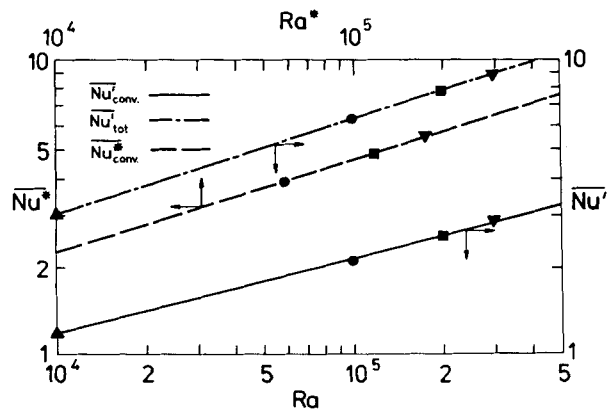

Figure 12. Average Nusselt number along the hot wall for all runs with external convection (primes denote values based on $T'_h - T'_a$)

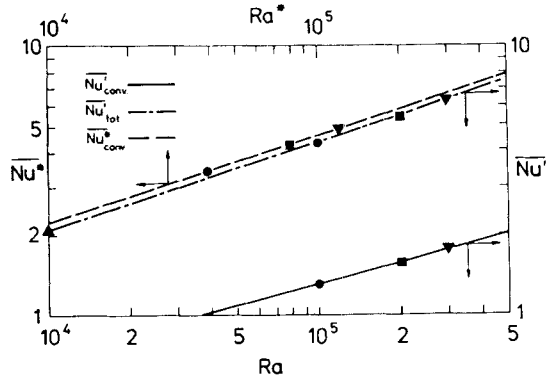

Figure 13. Average Nusselt number along the hot wall for all runs without external convection

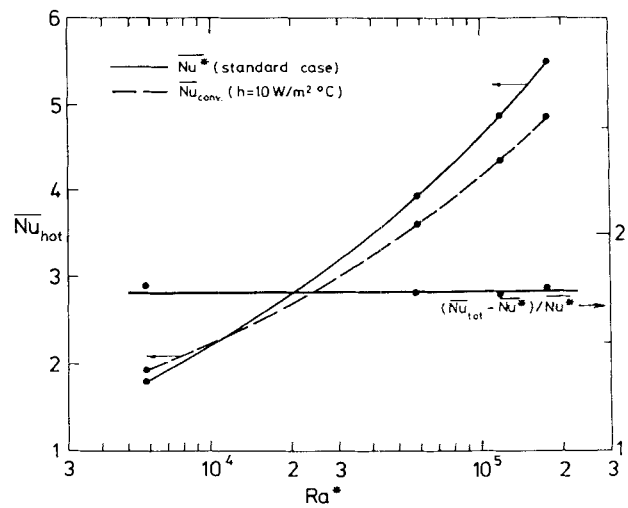

Figure 14. . Average Nusselt number along the hot wall based on $T'_h - T'_c$

The average convection Nusselt number based on $T'_h - T'_c$, for the runs which include radiative effects and external convection ($h = 10\ \mathrm{W\ m^{-2}\ °C^{-1}}$), is plotted in Figure 14. The average hot wall Nusselt number for the corresponding isothermal case is also given in this figure for comparison. The difference between the two calculated Nusselt numbers is the error in the predicted convective heat transfer which would have been made if an isothermal cold window temperature had been assumed (this temperature is not known *a priori*). Such an assumption leads to an underestimation of the convective heat transfer at low Rayleigh numbers ($Ra^* < 10^4$). However, a progressively increasing overprediction results at higher Rayleigh numbers. For instance, at an effective cavity Rayleigh number of $1{\cdot}2 \times 10^5$ the isothermal case yields an error of 12% in the convective heat transfer rate. Of course, the error in the total heat transfer (convection and radiation) is much higher if the standard model is used (the difference between these two Nusselt numbers is also plotted in Figure 14). This error is about 173% for the range of Rayleigh numbers considered here. In other words, for the problem simulated here, if the Nusselt numbers are calculated for the standard isothermal case they must be multiplied by 2·73 to yield the total heat transfer rate from the hot wall.

CONCLUSIONS

A numerical method for the study of combined natural convection and radiation in a rectangular, two-dimensional cavity containing a non-participating (i.e. transparent) fluid has been presented. One wall of the cavity was taken to be semitransparent (i.e. its transmissivity is less than unity). Expressions for view factors between area elements on the boundaries were derived so that local radiosities could be computed and detailed radiation calculations combined with natural convection calculations. A consideration of convection from the outside of the semitransparent boundary has also been incorporated.

Results have been presented for a square cavity with a vertical hot wall at 150 °C, an ambient temperature of 20 °C and $10^4 \leq Ra \leq 3 \times 10^5$, in the absence of direct insolation. The ways in which radiation and/or external convection affect the flow and heat transfer in the cavity have been revealed for this particular situation. In general terms it has been shown that external convection weakens the internal circulation, radiation strengthens it, and in combination—at least for the parameter values used here—the overall effect is a strengthening of the internal circulation.

ACKNOWLEDGEMENTS

Partial financial support from the Australian Research Grants Scheme is gratefully acknowledged. We thank Dr. S. S. Leong for his assistance in the early stages of this work.

APPENDIX: NOMENCLATURE

D'	cavity width
F	view factor
g	gravitational acceleration
h	convective heat transfer coefficient
J'	radiosity
k	thermal conductivity
K	configuration factor
L'	cavity height
L	cavity aspect ratio, L'/D'
n	co-ordinate normal to a surface
Pr	Prandtl number, ν/κ
q'	heat flux
Ra	Rayleigh number, $g\beta(T'_h - T'_a)D'^3/\nu\kappa$
t	time
T	temperature
u, v	x, y velocity components
x, y	co-ordinate directions
z	a point on any cavity wall
α	absorptivity
β	volumetric expansion coefficient
ε	emissivity
ζ	vorticity
θ	dimensionless temperature
κ	thermal diffusivity

ν	kinematic viscosity
ρ	reflectivity
σ	Stefan–Boltzmann constant
ϕ	cavity inclination to the vertical
ψ	streamfunction

Subscripts

a	ambient
c	cold wall
e	emitted radiation
h	hot wall
i	inside of the cold wall
l	long-wave radiation
o	outside of the cold wall
s	short-wave radiation
w	wall

Primes denote dimensional quantities (for clarity, these have been omitted from the symbols for material properties).

REFERENCES

1. S. Ostrach, 'Natural convection in enclosures', *Adv. Heat Transfer*, **8,** 161–227 (1972).
2. S. Ostrach, 'Natural convection heat transfer in cavities and cells', *Heat Transfer 1982, Vol. 1*, Hemisphere, Washington DC, 1982, pp. 365–379.
3. I. Catton, 'Natural convection in enclosures', *Proc. 6th Int. Heat Transfer Conf.*, Toronto, Vol. 6, 1979, pp. 13–43.
4. J. N. Arnold, I. Catton and D. K. Edwards, 'Experimental investigation of natural convection in inclined rectangular regions of differing aspect ratios', *J. Heat Transfer*, **98,** 67–71 (1976).
5. K. G. T. Hollands, T. E. Unny, G. D. Raithby and L. J. Konicek, 'Free convection heat transfer across inclined air layers', *J. Heat Transfer*, **98,** 189–193 (1976).
6. K. R. Randall, J. W. Mitchell and M. M. El-Wakil, 'Natural convection heat transfer characteristics of flat plate enclosures', *J. Heat Transfer*, **101,** 120–125 (1979).
7. S. M. ElSherbiny, G. D. Raithby and K. G. T. Hollands, 'Heat transfer by natural convection across vertical and inclined air layers', *J. Heat Transfer*, **104,** 96–102 (1982).
8. J. W. Elder, 'Laminar natural convection in a vertical slot', *J. Fluid Mech.*, **23,** 77–98 (1965).
9. C. M. Vest and V. S. Arpaci, 'Stability of natural convection in a vertical slot', *J. Fluid Mech.*, **36,** 1–15 (1969).
10. J. E. Hart, 'Stability of the flow in a differentially heated inclined box', *J. Fluid Mech.*, **47,** 547–576 (1971).
11. G. L. Morrison and V. Q. Tran, 'Laminar flow structure in vertical free convective cavities', *Int. J. Heat Mass Transfer*, **21,** 203–213 (1978).
12. N. Seki, S. Fukusako and H. Inaba, 'Visual observations of natural convective flow in a narrow vertical cavity', *J. Fluid Mech.*, **84,** 695–704 (1978).
13. W. M. M. Schinkel, 'Natural convection in inclined air-filled enclosures', *Ph.D. Thesis*, Delft University of Technology, 1980 (ISBN 90 6231 079 6).
14. G. de Vahl Davis and I. P. Jones, 'Natural convection in a square cavity: a comparison exercise', *Int. j. numer. methods fluids*, **3,** 227–248 (1983).
15. D. W. Larson and R. Viskanta, 'Transient combined laminar free convection and radiation in a rectangular enclosure', *J. Fluid Mech.*, **78,** 65–85 (1976).
16. D. W. Larson, 'Enclosed radiation and turbulent natural convection induced by a fire', in R. W. Lewis, K. Morgan and O. C. Zienkiewicz (eds), *Numerical Methods in Heat Transfer*, Wiley, 1981, pp. 467–487.
17. J. R. Lloyd, K. T. Yang and V. K. Lin, 'A numerical study of one-dimensional surface, gas, and soot radiation for turbulent buoyant flows in enclosures', *Proc. First Natl. Conf. on Numerical Methods in Heat Transfer*, 1979, pp. 142–161.
18. L. C. Chang, K. T. Yang and J. R. Lloyd, 'Radiation–natural convection interactions in two-dimensional complex enclosures', *J. Heat Transfer*, **105,** 89–95 (1983).
19. G. Lauriat, 'A numerical study of a thermal insulation enclosure: influence of the radiative heat transfer', presented at *19th Natl Heat Transfer Conf.*, ASME Publ. HTD Vol. 8, 1980, pp. 63–71.

20. B. Roux, J. C. Grondin and P. Bontoux, 'Natural convection in inclined rectangular cavities', *Proc. First Int. Conf. on Numerical Methods in Thermal Problems*, 1979, pp. 423–432.
21. G. D. Mallinson and G. de Vahl Davis, 'The method of the false transient for the solution of coupled elliptic equations', *J. Comput. Phys.*, **12**, 435–461 (1973).
22. E. M. Sparrow and R. D. Cess, *Radiation Heat Transfer*, Brooks/Cole Publishing, Belmont, CA, 1966.
23. A. A. Samarskii and V. B. Andreyev, 'On a high accuracy difference scheme for elliptic equations with several space variables', *USSR Comput. Math. Math. Phys.*, **3**, 1373–1382 (1963).
24. L. C. Woods, 'A note on the numerical solution of fourth order differential equations', *Aero. Q.*, **5**, 176–184 (1954).
25. G. de Vahl Davis, 'Natural convection of air in a square cavity: a bench mark numerical solution', *Int. j. numer. methods fluids*, **3**, 249–264 (1983).